Detecting Subpixel Woody Vegetation in Digital Imagery Using Two Artificial Intelligence Approaches

Patricia G. Foschi and Deborah K. Smith

Abstract

Small strips or patches of woody vegetation, typical landscape elements in many farming areas, are frequently not detected by standard computer-assisted classification of digital satellite imagery because such landscape elements are smaller than the pixel size and are mixed with other classes. This study essentially compares two artificial intelligence approaches—machine-vision and neural-network methods—developed to improve classification accuracy for this mixed pixel problem. Simulated multispectral and panchromatic SPOT HRV imagery of lowland Britain was used to test both methods. Compared to standard supervised multispectral classification, both methods yield significant improvements in detecting subpixel woody vegetation. In general, the machine-vision approach outperformed the neural-network approach. However, because each method generated different types of misclassifications, a classification map representing only the woody vegetation found by both methods provided the results with the least amount of overall error.

Introduction

Hedgerows and other woodland fragments are familiar elements in agricultural landscapes in Europe and the eastern part of North America. Such woody elements may be forest remnants or planted treerows; they may grow spontaneously or be intensely managed. In any case, in many agricultural settings such woody vegetation constitutes the primary wildlife nesting and feeding habitat. The distributions of birds and mammals are related to the shape, size, and spatial arrangement of these woody elements (Baudry, 1984; Forman and Godron, 1986). Monitoring these elements and quantifying changes are necessary for effective land-use planning and wildlife habitat management.

Small strips or patches of woody vegetation are usually subpixel targets, landscape elements smaller than the pixel size, in digital satellite imagery. Such small woody elements are often not detected by standard multispectral classification because the spectral values of mixed pixels containing these woody elements frequently do not match the spectral values of woody vegetation. Because standard multispectral classifiers operate on single pixels, they ignore spatial information in the data. Mixed pixels and indeed all pixels are treated as pure picture elements, which repeatedly results in mixed pixels being assigned to constituent or extraneous land-cover classes.

Figure 1 illustrates this problem for a two-band case. Figure 1(a) is a map of ground cover showing the locations of four mixed pixels, labeled A, B, C, and D. Each of these pixels contains two or three land-cover classes. Figure 1(b) represents a hypothetical two-dimensional feature space, created by plotting near-infrared digital numbers (DNs) against the corresponding red DNs. The five ellipses in Figure 1(b) are training set clusters, four representing the land-cover classes in Figure 1(a) and one representing an extraneous class, Crop 3. The four mixed pixels in Figure 1(a) are also plotted in Figure 1(b). Although the mixed pixels do not fall in any of their constituent training sets, a Euclidean nearest-neighbor classifier would place pixel A in one of its constituent classes, Fallow Land, and pixel D in one of its constituent classes, Crop 2. Pixel C has the same spectral response as Crop 3, the extraneous class. All standard multispectral classification techniques, from the simple box classifier to the more sophisticated maximum-likelihood classifier, would place pixel C in Crop 3. None of the mixed pixels is sufficiently close to the Various Trees cluster to be placed in this class. Different mixtures of classes produce mixed pixels scattered throughout the feature space. The same lack of separation occurs in the three-dimensional imagery used in this study.

An automated method for detecting subpixel woody vegetation in digital satellite imagery could provide an efficient means for mapping and monitoring woody vegetation and for quantifying shape, size, and spatial information of use to ecologists and resource managers. In this paper, two artificial intelligence (AI) strategies were employed to detect subpixel woody vegetation: (1) a rule-based scheme based on a machine-vision approach and (2) a neural network trained with a back-propagation learning algorithm.

Background

A rule-based classification scheme organizes a set of decision rules into one classification strategy. Such classification schemes operate as a series of separate decisions and generate datasets at each stage in the process. In theory, any combination of image-processing techniques may be incorporated. Rule-based classification systems encompass a considerable variety of algorithms. Among the plethora of algorithms, simple cases of rule-based schemes are called layered classifiers. A layered classifier may be simply the application of two multispectral classification methods in tandem. For example, Mather (1987) describes the use of the box classifier to identify well-separated classes followed by the use of the maximum-likelihood classifier to discriminate the more difficult

Department of Geography and Human Environmental Studies, San Francisco State University, 1600 Holloway Avenue, San Francisco, CA 94132.

Photogrammetric Engineering & Remote Sensing, Vol. 63, No. 5, May 1997, pp. 493–500.

0099-1112/97/6305-493$3.00/0

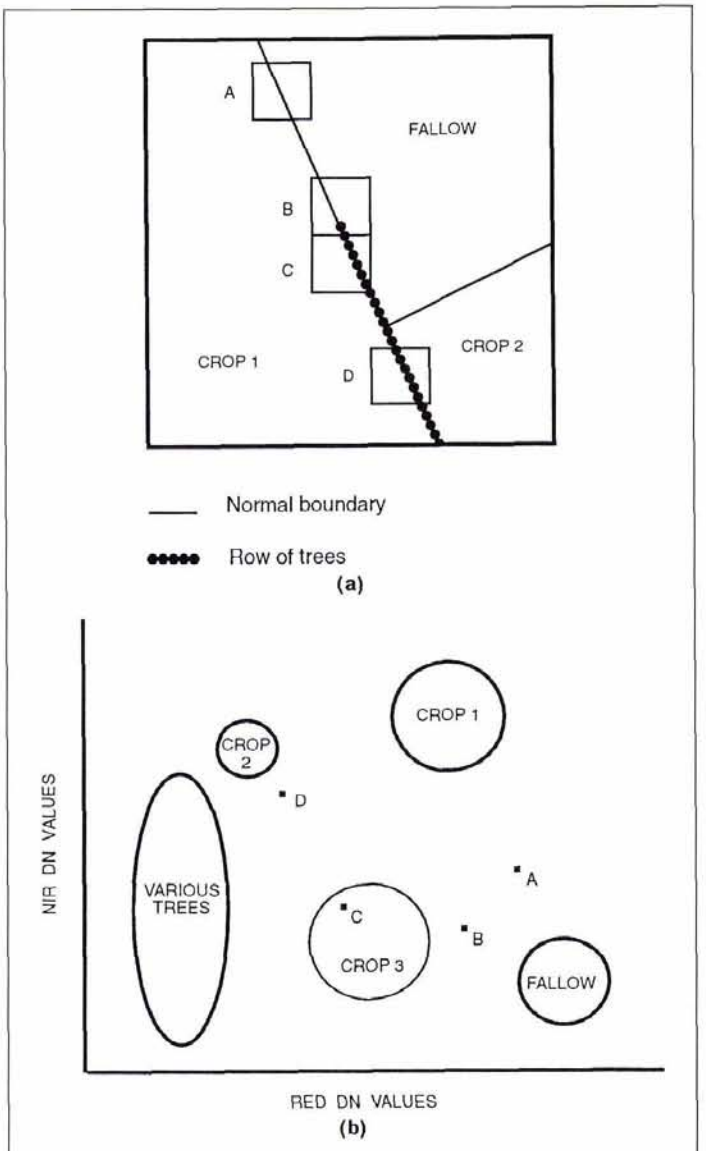

Figure 1. Four mixed pixels located on the ground and in feature space. (a) Map of ground cover showing locations of four mixed pixels, labeled A, B, C, and D. (b) Two-dimensional feature space. The ellipses represent locations of five training sets or classes.

or overlapping classes. On the other hand, a rule-based system may be a large and complex set of programs functioning as an expert system that simulates the higher-order interpretative processes of human analysts. For example, Nagao and Matsuyama (1980) developed one of the first expert systems for analyzing digital imagery. Their rule-based system classifies land cover in high-resolution scan-digitized aerial photographs. This system incorporates edge-preserving smoothing, segmentation, texture analysis, structural descriptions of pattern, multispectral classification, measures of elongatedness, size descriptions for objects, and decision-tree logic. Argialas (1990) provides a review of rule-based AI techniques for capturing and representing a photointerpreter's expertise in pattern recognition. When such knowledge representation imitates or simulates the logic of human perception, it is called machine or computer vision.

A number of rule-based algorithms explicitly address mixed pixel problems. For example, Enslin *et al.* (1987) integrated Landsat Thematic Mapper (TM) imagery and ancillary data in a rule-based system to detect new oil and gas wells within forests. Key *et al.* (1990) developed a rule-based classifier to map sea ice leads from a transparency of a Landsat MSS Band 4 (near-infrared) image, scan-digitized to a pixel size of 200 m.

Training a neural network is essentially an opposite endeavor from devising a rule-based classification scheme. Back-propagation neural networks are designed to function as general pattern-recognition algorithms. Such algorithms perform a specific task only after training has been successful. Training a back-propagation neural network does not require *a priori* knowledge of the mathematical relationships that constitute a rule-based classification system.

Since the publication of Rumelhart and McClelland (1986), there has been a renaissance of interest in using neural networks, particularly back-propagation neural networks, for image classification. A back-propagation neural network is particularly suitable for image classification because it supports supervised training of preprocessed multivariate data. Some of the successful back-propagation neural network applications include the classification of Landsat MSS imagery (McClellan *et al.*, 1989; Benediktsson *et al.*, 1990), of Landsat TM imagery (Howald, 1989; Hepner *et al.*, 1990; Heermann and Khazenie, 1992), and of SPOT HRV imagery (Kanellopoulos *et al.*, 1992; Dreyer, 1993).

Only a few researchers have investigated using neural networks as tools for addressing mixed pixel problems. For example, back-propagation neural networks have been used to locate linear features. Ryan *et al.* (1991) successfully delineated shorelines in high-resolution scan-digitized aerial photography using a combination of neural-network and traditional image-processing procedures. Penn *et al.* (1993) attempted to detect geologic edges and linear features, like faults and lineaments, in TM data. They concluded that neural networks are of only limited use for distinguishing linear features, but are capable of detecting edges at various scales. Boggess (1994) found that integrating contextual or spatial information into a back-propagation neural network was necessary to locate roads in TM imagery.

Study Sites and Data

The study area is located southeast of the city of Winchester, in southern England, in an area of mixed farmland and woodland. This region, typical of agricultural lands in lowland Britain, contains numerous small woody elements and farm fields arranged in "patchwork-quilt" patterns. The majority of the woody vegetation is deciduous. Like surrounding areas of Hampshire, the study area is a chalkland in a gently rolling terrain.

Simulated SPOT HRV imagery, flown on 6 July 1984, was available for the study. Panchromatic and multispectral bands were simulated using Daedalus DS-1268 scanner Bands 3 through 7 singly or in combination. The wavelength intervals of the bands approximate those of real SPOT imagery. The spatial resolutions—20 m in the three multispectral bands and 10 m in the panchromatic band—match those of real SPOT imagery at nadir viewing.

Two types of preprocessing were necessary: geometric correction and radiometric adjustments. The panchromatic and multispectral data were not registered to one another because they were collected during different flights. In order to fit the panchromatic data to the other bands precisely, it was necessary to divide the panchromatic data into smaller pieces. Due to the small sizes of the features of interest, the precision of the geometric correction was judged by overlaying the imagery on a monitor rather than by statistical measures. The four subsites, called WS1 through WS4, resulting

Figure 2. Panchromatic band for subsite WS3.

from this process represent areas containing only perfectly registered linear features. Resampling was calculated by the nearest-neighbor method. Because all of the simulated bands were collected as 8-bit data, reduction of the gray-tone range was needed to better approximate the SPOT panchromatic band. The 8-bit panchromatic data were changed to 6-bit data by simply combining every four DNs into one unit.

The presence of woody vegetation within the sites was interpreted from 1:10,000-scale panchromatic aerial photography, flown on 28 July 1984. The locations of single trees, single rows of trees, and denser strips and patches of woody vegetation were mapped into digital images using the multispectral data as a template. Woody elements less than two metres in width were not included, and species of vegetation were not identified. Airphoto interpretations were partially checked by ground surveys.

The four subsites constitute 19922 pixels. Only illustrations for subsites WS3 and WS4 are included in this paper. The panchromatic band for subsite WS3, the largest of the subsites, is reproduced in Figure 2. Ground data maps are depicted in Figure 3, in which black pixels represent woody vegetation. Subsite WS3 contains some of the smallest farm fields in the study, and subsite WS4 contains the most reflective fallow fields. The linear woody elements in these sites range from hedges about one metre wide to belts several trees wide. Deciduous patches, scrubland, conifers, main roads, farm lanes, and buildings are also present.

The Rule-Based Machine-Vision Approach

During a previous study, a rule-based classification scheme was developed specifically to detect woody vegetation in simulated SPOT HRV imagery (Foschi, 1992). This scheme incorporates two automated classification steps and two automated procedures for integrating image-derived masks into the decision process. The overall scheme, shown in Figure 4, involves several stages before the map of total woody vegetation is generated in the final stage.

The input datasets, which constitute the first stage in Figure 4, are the four simulated SPOT bands: green (G), red (R), near-infrared (NIR), and panchromatic (PAN). All subsequent datasets are derived from these four.

The first dataset in the second stage, Large Woody, is the map of woody vegetation produced by the first classification step. This step locates large patches of woodland by a standard multispectral classifier using the three multispectral bands. The nearest-neighbor classifier—using Mahalanobis distances and nine training classes derived from 18 training sites—was used in this study, but another supervised classification method could be substituted.

The PMASK dataset, the next dataset in the second stage, is generated from the panchromatic band and is the output map of a local-difference filter. This filter was designed specifically to detect locally darker pixels and to create a mask that marks these pixels for further processing. Because small woody elements, including many hedges only one metre wide, are consistently detectable as darker shapes in the panchromatic band, the pixels marked in this mask represent potential woody vegetation. Relative darkness is calculated by comparing the central pixel of a 5 by 5 window with the means of four pairs of outer pixels. Because the PMASK dataset consists of 10-m pixels, it was necessary to combine the information in every 2 by 2 array to produce 20-m marked pixels compatible with the multispectral data. The 20-m version of PMASK is the MASK1 dataset, which occurs in the third stage in Figure 4. Figure 5 depicts the MASK1 datasets for subsites WS3 and WS4.

The last dataset in the second stage, the NDVI dataset, is a map of normalized difference vegetation indices, calculated from the red and near-infrared bands. This vegetation index is defined by the following formula:

$$\text{NDVI} = \frac{\text{NIR} - \text{R}}{\text{NIR} + \text{R}}$$

The MASK2 dataset in the third stage is derived from the NDVI dataset. This mask delineates both the darkest NDVI values, all values less than or equal to zero, and the locally

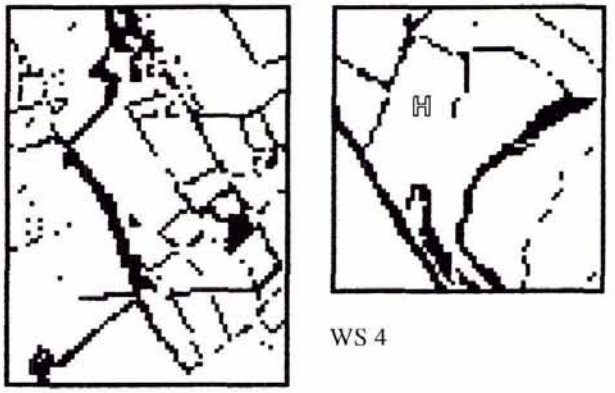

WS 4

WS 3

Figure 3. Ground data maps for subsites WS3 and WS4. Black pixels represent woody vegetation greater than two metres in width. One smaller woody element, a 1-m wide hedgerow, occurs at location marked with an outlined H.

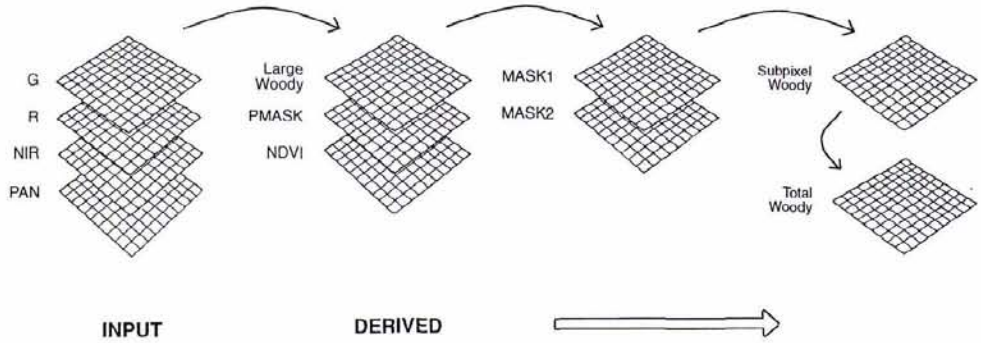

Figure 4. Overall scheme showing five stages of rule-based method. G, R, NIR, and PAN are the four simulated SPOT bands, from which all other datasets are derived.

darker values, output from the local-difference filter. The MASK2 dataset represents unvegetated pixels.

The second classification step creates the Subpixel Woody map, the dataset in the fourth stage in Figure 4. This step uses the red and near-infrared bands and the MASK1 and MASK2 datasets to detect subpixel woody vegetation. The classification method relies on an 11 by 1 moving window, passed horizontally and vertically over the two spectral bands, to collect training sets for adjacent land cover and to analyze mixture phenomena at the individual pixel level. Figure 6 illustrates two of the 14 moving-window configurations tested during the development of the method; the 11 by 1 window yielded the best classification results. In each case, the window is partitioned into three functional regions: two training sets for the adjacent farm fields and a central region expected to contain mixed pixels. The analysis of mixture phenomena is based on the construction and division of two-dimensional feature spaces derived from window data. Figure 7 shows the conceptual divisions of a typical feature space. In this figure, the squares represent a woody vegetation training set, which is also the deciduous woodland training set employed in the first classification step described above. The dels and deltas represent the training sets in a particular 13 by 3 window, the central pixel of which is identified by the line and sample numbers given, and the circles represent potential mixed pixels from the central region of this window. The dashed line in Figure 7 is the preliminary division line that partitions the feature space into two classification zones, potentially woody and non-woody zones. The solid line is the final division line, which is the preliminary division line shifted three DN values closer to the woody vegetation training set to decrease the possibility of misclassification. When pixels from the central region of the window contain a small woody element, these pixels are expected to fall in the potentially woody zone, on the woody cluster side of the division line. The circles on the woody cluster side of the division line in Figure 7 are, in fact, pixels containing trees. Identifying a potential mixed pixel by its spatial position and then locating it in the woody zone is the basis for classifying it as subpixel woody vegetation. At each window position, the feature-space configuration and the location of the division line vary with the spectral locations of the non-woody training sets. Using a computer to identify the feature-space configuration, to calculate the division line, and to discriminate mixed pixels expected to contain woody vegetation is essentially a machine-vision problem. Two papers, by Foschi (1992) and Foschi (1994), relate further details of the method developed to allow a computer to "see" the lines and the relationships.

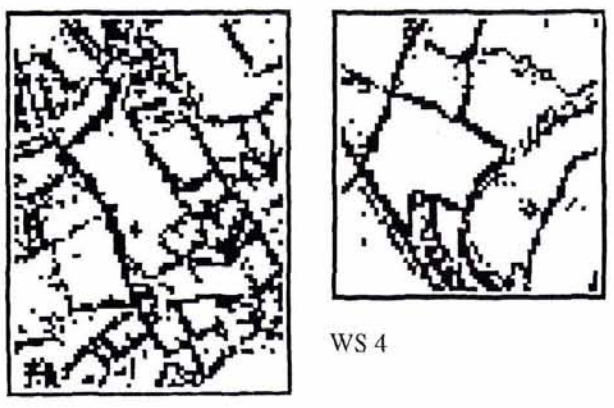

WS 3

WS 4

Figure 5. MASK1 datasets for subsites WS3 and WS4. Black pixels represent potential woody vegetation.

The two masks are incorporated into this second classification step in order to locate pixels of interest and to decrease noise. Data for a particular window are accepted for analysis only when the central pixel of the window corresponds to a marked pixel in the MASK1 dataset, a pixel potentially containing woody vegetation. The MASK2 dataset is employed to locate mixed pixels containing non-woody subpixel targets, like buildings and roads. Pixels identified as unvegetated in this mask are not classified as subpixel woody vegetation.

In the fifth stage of Figure 4, the Total Woody dataset is created. Because the second classification step does not distinguish large woody patches, the two classification steps are needed to map both large patches and subpixel fragments of woody vegetation. The resultant classification maps, the Large Woody and Subpixel Woody datasets, are added together to yield the Total Woody dataset. Figure 8 shows the maps of total woody vegetation for subsites WS3 and WS4.

The Neural-Network Approach

In this study, a neural network was trained to detect subpixel woody vegetation. BrainMaker™ 2.5, software for IBM-compatible PCs, was used to simulate a feed-forward multilayer perceptron trained with a back-propagation learning algorithm.

The final version of the neural-network architecture, illustrated in Figure 9, consists of three layers: eight input variables or units, 18 hidden units, and one output variable or

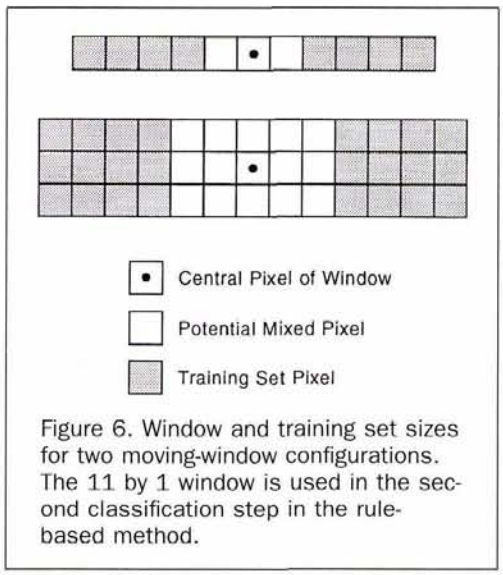

Figure 6. Window and training set sizes for two moving-window configurations. The 11 by 1 window is used in the second classification step in the rule-based method.

unit. The network is fully connected and contains one bias unit. The sigmoidal function, the most commonly used in back-propagation neural networks, is incorporated as the firing function, and the default gain of 1.0 is used.

The eight input variables include six datasets used in the machine-vision method: the simulated multispectral bands (G, R, and NIR), the NDVI values, and the two masks (MASK1 and MASK2). The panchromatic band was resized to match the 20-m pixel size by reading every 2 by 2 array in the panchromatic data and assigning the darkest value in the array to an output band. This process created the PANDK dataset. The NIR/R band ratio was included as an input variable because its presence during the trial runs appeared useful. Its inclusion is also intuitively appealing because this variable gives a rough indication of position in the two-dimensional feature space, a characteristic that reflects some of the logic of the machine-vision approach. The NDVI values and the NIR/R ratios were calculated within BrainMaker™ in order to retain real values and the maximum number of decimal places. The output variable represents the presence or absence of woody vegetation.

Training Considerations

The particular network reported upon here is the result of dozens of trial runs performed on various architectures. This network was judged to be the best by both training and test accuracy assessments and by visual inspection of the output classification maps. The numbers of input, hidden, and output units and the types of input and output variables were modified during these trials. Up to 15 raw and derived variables were used as input variables. Trial architectures with and without spatial datasets—i.e., three texture bands generated from the multispectral data and the two masks used in the machine-vision method—were tested. Because this version of BrainMaker™ does not support self-pruning, the effective number of hidden units was determined from a series of trial runs in which only the number of hidden units was varied. Both one and four output variables were attempted. As mentioned above, the single output variable represented the presence or absence of woody vegetation. The four outputs represented the coarse land-cover classes occurring in the study sites: woodland, dark cropland, bright cropland/pasture, and bare soil. Discriminating crop classes was not attempted. This list of variations in architecture is by no means exhaustive, and some avenues of investigation—for example, the use of multiple output units and their potential for proportion estimation—need further study.

In contrast to traditional practice, both "pure" and mixed pixels were selected to train the neural network. Only pure pixels were selected for training in the multispectral classification and the machine-vision methods. Training with one whole subsite and training with selected pixels were tested. The final network was trained with input and output variables for 1627 pixels: approximately 5 percent pure woodland, 70 percent pure other land cover, 16 percent subpixel woody vegetation, and 9 percent other mixtures. Small strips of woody vegetation adjacent to the various other land cover and larger patches of woodland and of dark cropland were particularly well represented by these samples.

The BrainMaker™ defaults for the training parameters were used: randomly initiated weights, a learning rate of one, a learning tolerance of 0.1, a testing tolerance of 0.4, and a momentum of 0.9 (California Scientific Software, 1992). Regional, rather than training-set specific, minima and maxima were used to normalize the data. The number of iterations for training, 142, corresponded to the point at which the highest percentage correct occurred during training. The highest percentage correct was approximately 83 percent. Any significantly longer training time decreased the percentage correct; convergence never occurred.

Three techniques have been suggested for increasing the generalizing ability of a network (Dayhoff, 1990; Lawrence, 1993): (1) pruning the hidden units, (2) adding noise while training, and (3) changing the input variables. The goal in selecting various units is to find a network large enough to learn the task, but small enough to generalize (Hammerstrom, 1993). Because the version of BrainMaker™ used in

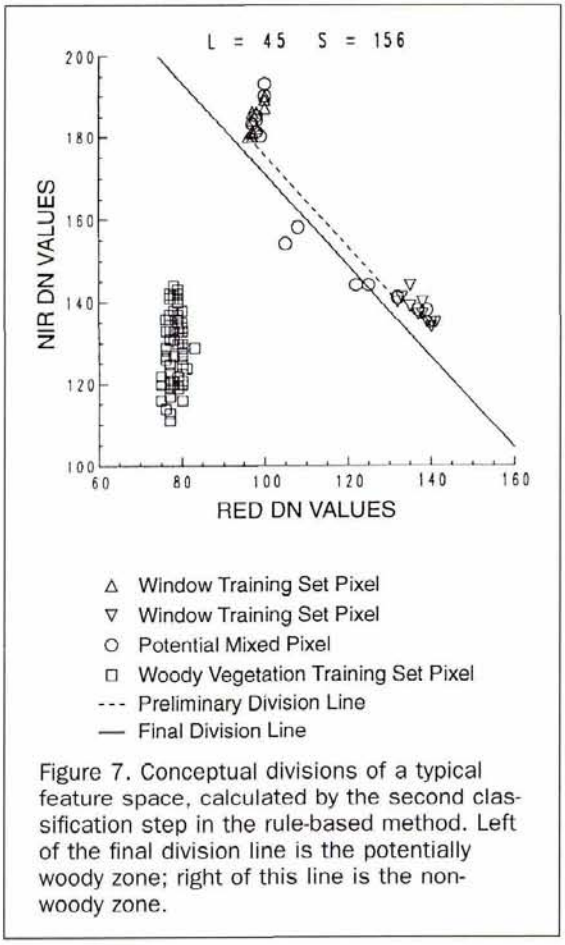

Figure 7. Conceptual divisions of a typical feature space, calculated by the second classification step in the rule-based method. Left of the final division line is the potentially woody zone; right of this line is the nonwoody zone.

this study does not permit partially connecting layers or permanently setting weights equal to zero, pruning hidden units was not possible. The mixed pixels that represent subpixel woody vegetation constitute a very noisy dataset; using noise with very noisy data is not recommended (Lawrence, 1993). Indeed, adding noise was found to be counter-productive and resulted in output maps showing virtually no woody vegetation.

Modifying the input variables was productive. Trial runs contained as few as three and as many as 15 input variables. While not every possible combination was tried, the eight variables selected for the final network were repeatedly found to be useful in the trials.

Results and Discussion

The final network was used to classify subsites WS1 through WS4 and resulted in output maps representing the continuum from non-woody to woody as decimal values from 0.0000 to 1.0000, respectively. These values, treated here as "probabilities," were converted to maps of woody vegetation by density slicing. Cut-off points at various probability levels were tried. Table 1 summarizes the accuracy assessment for woody vegetation in the output maps using various cut-off points. The output maps for the 0.85 probability level are shown in Figure 10. These maps were selected for comparison because their errors of commission are closest to those errors produced by the machine-vision method.

A summary of the accuracy assessment for all methods is given in Table 2. In all cases, the outer four rows and columns in the classification and ground data maps have been dropped from consideration because the window shape in the machine-vision method does not permit complete processing of these areas. The remaining 15642 pixels in subsites WS1 through WS4 have been tabulated.

The overall percentages of error and accuracy, shown in Table 2, are not remarkably different for the various methods because the Winchester subsites are dominated by non-woody land cover. However, the classification of woody vegetation changes significantly. While the standard multispectral method correctly classified 24.1 percent of the woody vegetation, the machine-vision method found 65.1 percent and the neural-network method found 56.5 percent of this vegetation. Both AI methods produce maps with relatively large errors of commission. Generally, the machine-vision method outperforms the neural-network method because it detects more woody vegetation while it generates similar errors of commission.

A number of the errors exhibited by the machine-vision method are due to registration problems and mapping anomalies. For example, the machine-vision method tends to produce linear woody elements wider or thinner than the hand-drawn elements on the ground data maps; these differences produce larger estimates of error. The detected hedgerow in subsite WS4 in Figure 8, corresponding to the woody element labeled H in Figure 3, is not present in the ground data map because it is less than two metres in width. Consequently, the pixels of the hedgerow are counted as errors of commission in the machine-vision method. The length of the 11 by 1 moving window may also produce anomalous classifications. Negotiating small fields or linear landscape elements intersecting at acute angles may cause omitted or irregularly shaped woody elements.

On the other hand, the neural network, essentially a point operator, demonstrated greater difficulty locating woody vegetation without spatial data. The two masks, developed to reduce noise and decrease processing time in the machine-vision method, are indispensable input variables to the neural network. Although adding and removing some variables made little difference, only architectures containing the two masks yielded any significant results. Architectures

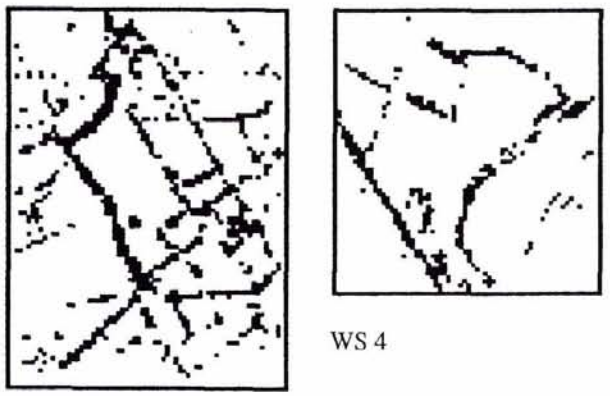

WS 4

WS 3

Figure 8. Total woody vegetation, mapped by the rule-based method, in subsites WS3 and WS4. Black pixels represent woody vegetation.

that did not contain the two masks created maps with virtually no woody vegetation. Omission of the masks from the machine-vision method does not reduce accuracy as conspicuously.

The two AI methods generate different types of misclassification. The machine-vision method confuses increased soil moisture and/or relief with woody vegetation and generates speckled areas when more highly textured or highly patterned land cover is present. As a point operator, the neural network appears to draw shapes more accurately and is much less confused by highly textured and highly patterned areas. The neural network frequently confuses "dark red" cropland with woody vegetation. Dark red here refers to the color of the cropland in standard false-color IR composites. The linear elements in MASK1, depicted in Figure 5, that the neural network misclassifies as woody vegetation in Figure 10 are the boundaries of red fields. As the probability level decreases in Table 1, the errors of commission increase, pre-

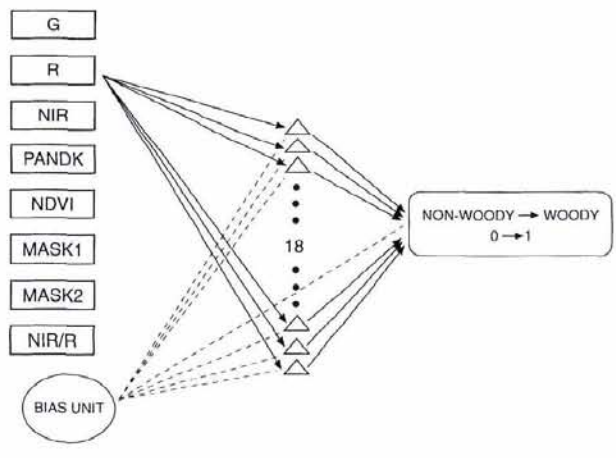

Figure 9. Neural-network architecture. The network is fully connected; but, for clarity, many of the connections have been omitted.

TABLE 1. SUMMARY OF ACCURACY ASSESSMENT FOR WOODY VEGETATION IN THE CLASSIFICATION MAPS GENERATED BY THE NEURAL NETWORK.

Probability level for density slicing	Errors of omission	Errors of commission	Percent correct
0.90	52.1	14.0	47.9
0.89	50.4	16.5	49.6
0.88	48.1	19.0	51.9
0.87	47.0	21.1	53.0
0.86	45.3	23.2	54.7
0.85	43.5	25.9	56.5
0.84	41.8	28.9	58.2
0.80	36.7	41.7	63.3

dominantly due to the addition of red cropland including pixels not marked in MASK1.

Because these two AI approaches produced different types of misclassification, classification maps representing only the woody vegetation found by both methods were generated and evaluated. The accuracy assessment for two sets of these maps is also summarized in Table 2. If reducing errors of commission is the primary criterion for assessment, this composite mapping provides the most satisfactory results.

Summary and Conclusion

A rule-based machine-vision method was developed and a back-propagation neural-network method was employed to detect subpixel woody vegetation in simulated SPOT HRV imagery of lowland Britain. These methods represent virtually opposite approaches to image classification. While rule-based methods are designed to perform a specific task, back-propagation neural networks are designed to function as general pattern-recognition algorithms. A neural network performs a specific task only after training has been successful. Training a back-propagation neural network does not require *a priori* knowledge of the mathematical relationships that constitute a rule-based classification system.

The selection of training sets for the two methods also represents opposite approaches: pure samples are needed for the machine-vision method while both pure samples and mixtures are needed for the neural-network method. Because mixed pixels containing woody vegetation are scattered throughout feature space, aggregate statistics for these mixed pixels are roughly equivalent to statistics for the entire image. No traditional method can successfully utilize this information. The neural network, designed to discriminate complex patterns, was successfully trained only using mixtures.

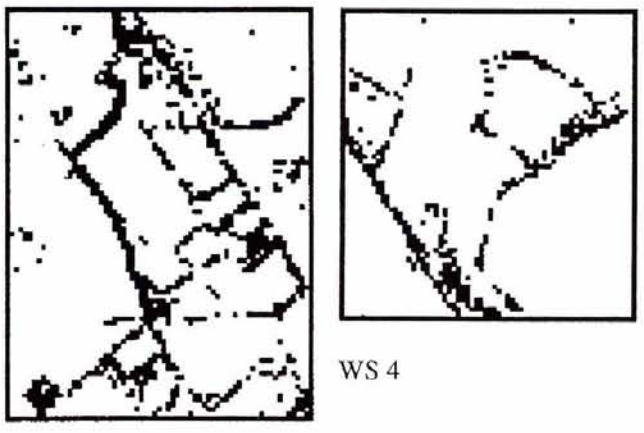

WS 4

WS 3

Figure 10. Woody vegetation, mapped by the neural network, in subsites WS3 and WS4. Black pixels mark probability levels of 0.85 or higher.

TABLE 2. SUMMARY OF ACCURACY ASSESSMENT FOR ALL METHODS.

Method	Class	Errors of omission	Errors of commission	Percent correct
Mahalanobis	non-woody	0.2	9.6	99.8
distance	woody	75.9	1.7	24.1
	overall	8.7	8.7	91.3
rule-based	non-woody	3.3	4.4	96.7
machine-vision	woody	34.9	26.5	65.1
	overall	6.9	6.9	93.1
neural-network at	non-woody	3.3	5.5	96.7
0.85 probability	woody	43.5	25.9	56.5
level	overall	7.8	7.8	92.2
composite using	non-woody	0.8	6.9	99.2
0.85 probability	woody	55.1	6.6	44.9
level	overall	6.9	6.9	93.1
composite using	non-woody	1.0	6.5	99.0
0.80 probability	woody	51.3	8.2	48.7
level	overall	6.7	6.7	93.3

Strategies for improving classification accuracy for the two methods are also different. For the rule-based machine-vision method, code may be implemented to correct identified problems. On the other hand, improving the output of the neural network is essentially a trial-and-error process. While input variables are somewhat correlated to the output variable, the relationships are nonlinear and complex. Presently, there is little theory to guide training strategies for back-propagation neural networks.

Both AI methods were tested using simulated multispectral and panchromatic SPOT HRV imagery for four subsites. The results suggest that both methods represent significant improvements in detecting subpixel woody vegetation when compared to standard supervised multispectral classification. Because the two approaches produced different types of misclassification, maps representing only the woody vegetation detected by both methods contained the least amount of overall error.

Acknowledgments

The imagery and other research materials were purchased with grants from two trust funds associated with the University of Oxford, the Vaughan Cornish Bequest and the St. Hilda's College Muriel Wise Fund. The figures were created with the help of Hugh Howard. Jeff Milliken and Jeff Simon interpreted the airphotos and digitized the ground data. The imagery was commissioned by the National Remote Sensing Centre in Farnborough, England, and flown by Hunting Geology and Geophysics Limited. The airphotos were flown by Meridian Airmaps Limited for the Planning Department of the Hampshire County Council.

References

Argialas, D.P., 1990. Knowledge-based image interpretation: techniques and applications, *Technical Papers of ACSM/ASPRS Annual Convention*, Denver, Colorado, 4:33–42.

Baudry, J., 1984. Effects of landscape structure on biological communities: the case of hedgerow network landscapes, *Proceedings of 1st International Seminar on Methodology in Landscape Ecological Research and Planning*, Roskilde, Denmark, International Association for Landscape Ecology, 1:55–65.

Benediktsson, J.A., P.H. Swain, and O.K. Ersoy, 1990. Neural network approaches versus statistical methods in classification of

multisource remote sensing data, *IEEE Transactions on Geoscience and Remote Sensing*, GE-28:540–552.

Boggess, J.E., 1994. Using artificial neural networks to identify roads in satellite images, *Proceedings of the World Congress on Neural Networks*, San Diego, California, 1:410–415.

California Scientific Software, 1992. *BrainMaker Neural Network Simulation Software: User's Guide and Reference Manual*, Nevada City, California.

Dayhoff, J.E., 1990. *Neural Network Architectures: An Introduction*, Van Nostrand Reinhold, New York, N.Y.

Dreyer, P., 1993. Classification of land cover using optimized neural nets on SPOT data, *Photogrammetric Engineering & Remote Sensing*, 59:617–621.

Enslin, W.R., J. Ton, and A. Jain, 1987. Land cover change detection using a GIS-guided, feature-based classification of Landsat Thematic Mapper data, *Technical Papers of ASPRS/ACSM Annual Convention*, Baltimore, Maryland, 6:108–120.

Forman, R.T.T., and M. Godron, 1986. *Landscape Ecology*, John Wiley and Sons, New York, N.Y.

Foschi, P.G., 1992. *Classification of Subpixel Woody Vegetation in Remotely-Sensed Imagery of Lowland Britain*, doctoral thesis, University of Oxford, UK.

———, 1994. A geometric approach to a mixed pixel problem: detecting subpixel woody vegetation, *Remote Sensing of Environment*, 50:317–327.

Hammerstrom, D., 1993. Working with neural networks, *IEEE Spectrum*, 30(7):46–53.

Heermann, P.D., and N. Khazenie, 1992. Classification of multispectral remote sensing data using a back-propagation neural network, *IEEE Transactions on Geoscience and Remote Sensing*, GE-30:81–88.

Hepner, G.F., T. Logan, N. Ritter, and N. Bryant, 1990. Artificial neural network classification using a minimal training set: comparison to conventional supervised classification, *Photogrammetric Engineering & Remote Sensing*, 56:469–473.

Howald, K.J., 1989. Neural network image classification, *Technical Papers of ASPRS/ACSM Fall Convention*, Cleveland, Ohio, pp. 207–215.

Kanellopoulos, I., A. Varfis, G.G. Wilkinson, and J. Megier, 1992. Land-cover discrimination in SPOT HRV imagery using an artificial neural network: a 20-class experiment, *International Journal of Remote Sensing*, 13:917–924.

Key, J., A.J. Schweiger, and J.A. Maslanik, 1990. Mapping sea ice leads with a coupled numeric/symbolic system, *Technical Papers of ACSM/ASPRS Annual Convention*, Denver, Colorado, 4: 228–237.

Lawrence, J., 1993. *Introduction to Neural Networks: Design, Theory, and Applications*, California Scientific Software, Nevada City, California.

Mather, P.M., 1987. *Computer Processing of Remotely-Sensed Images: An Introduction*, John Wiley and Sons, Chichester, UK.

McClellan, G.E., R.N. DeWitt, T.H. Hemmer, L.N. Matheson, and G.O. Moe, 1989. Multispectral image-processing with a three-layer backpropagation network, *Proceedings of International Joint Conference on Neural Networks*, Piscataway, New Jersey, IEEE, 1:151–153.

Nagao, M., and T. Matsuyama, 1980. *A Structural Analysis of Complex Aerial Photographs*, Plenum, New York, N.Y.

Penn, B.S., A.J. Gordon, and R.F. Wendlandt, 1993. Using neural networks to locate edges and linear features in satellite images, *Computers and Geosciences*, 19:1545–1565.

Rumelhart, D.E., and J.L. McClelland, 1986. *Parallel Distributed Processing*, MIT Press, Cambridge, Massachusetts, Vols. 1–2.

Ryan, T.W., P.J. Sementilli, P. Yuen, and B.R. Hunt, 1991. Extraction of shoreline features by neural nets and image processing, *Photogrammetric Engineering & Remote Sensing*, 57:947–955.

(Received 31 October 1994; accepted 19 October 1995; revised 17 April 1996)

Forthcoming Articles

Peter M. Atkinson *and* Paul J. Curran, *Choosing an Appropriate Spatial Resolution for Remote Sensing Investigations.*

Georges Blaha, *Accuracy of Plates Calibrated by an Automatic Monocomparator.*

Michel Boulianne, Clément Nolette, Jean-Paul Agnard, *and* Martin Brindamour, *Hemispherical Photographs Used for Mapping Confined Spaces.*

Roland J. Duhaime, Peter V. August, *and* William R. Wright, *Automated Vegetation Mapping Using Digital Orthophotography.*

Gary R. Clay *and* Stuart E. Marsh, *Spectral Analysis for Articulating Scenic Color Changes in a Coniferous Landscape.*

Christopher D. Elvidge, Kimberly E. Baugh, Eric A. Kihn, Herbert W. Kroehl, *and* Ethan R. Davis, *Mapping City Lights with Nighttime Data from the DMSP Operational Linescan System.*

Clyde C. Goad *and* Ming Yang, *A New Approach to Precision Airborne GPS Positioning for Photogrammetry.*

Luoheng Han, *Spectral Reflectance with Varying Suspended Sediment Concentrations in Clear and Algae-Laden Waters.*

Perry J. Hardin *and* J. Matthew Shumway, *Statistical Significance and Normalized Confusion Matrices.*

Robert L. Huguenin, Mark A. Karaska, Donald Van Blaricom, *and* John R. Jensen, *Subpixel Classification of Bald Cypress and Tupelo Gum Trees in Thematic Mapper Imagery.*

Kazuo Kobayashi *and* Chuji Mori, *Relations between the Coefficients in Projective Transformation Equations and the Orientation Elements of a Photograph.*

Miklos Kovats, *A Large-Scale Aerial Photographic Technique for Measuring Tree Heights on Long-Term Forest Installations.*

Rongxing Li, *Mobile Mapping—An Emerging Technology for Spatial Data Acquisition.*

D.D. Lichti *and* M.A. Chapman, *Constrained FEM Self-Calibration.*

Hans-Gerd Maas *and* Thomas Kersten, *Aerotriangulation and DEM/Orthophoto Generation from High Resolution Still-Video Imagery.*

Scott Mason, *Heuristic Reasoning Strategy for Automated Sensor Placement.*

Youngsinn Sohn *and* Roger M. McCoy, *Mapping Desert Shrub Rangeland Using Spectral Unmixing and Modeling Spectral Mixtures with TM Data.*

David M. Stoms, Michael J. Bueno, *and* Frank W. Davis, *Viewing Geometry of AVHRR Image Composites Derived Using Multiple Criteria.*

Paul Sutton, Dar Roberts, Chris Elvidge, *and* Henk Meij, *A Comparison of Nighttime Satellite Imagery and Population Density for the Continental United States.*

J.E. Vogelmann, T. Sohl, *and* S.M. Howard, *Regional Characterization of Land Cover Using Multiple Sources of Data.*

Lucien Wald, Thierry Ranchin, *and* Marc Mangolini, *Fusion of Satellite Images of Different Spatial Resolutions: Assessing the Quality of Resulting Images.*

Timothy A. Warner *and* Michael Shank, *An Evaluation of the Potential for Fuzzy Classification of Multispectral Data Using Artificial Neural Networks.*